ChemComm
Chemical Communications

Accepted Manuscript

This article can be cited before page numbers have been issued, to do this please use: X. Jiang, H. Li, Y. Shang, F. Wang, H. Chen, K. Xu, M. Yin, H. Liu, W. Zhou and Z. Ning, *Chem. Commun.*, 2019, DOI: 10.1039/C9CC04157E.

ROYAL SOCIETY OF CHEMISTRY

rsc.li/chemcomm

View Article Online
DOI: 10.1039/C9CC04157E

COMMUNICATION

Bi-Inorganic-ligands Coordinated Colloidal Quantum Dot Ink

Xianyuan Jiang,[a‡] Hansheng Li,[a‡] Yuequn Shang,[a] Fei Wang,[a] Hao Chen,[a] Kaimin Xu,[a] Ming Yin,[a] Hefei Liu,[b] Wenjia Zhou,[a] and Zhijun Ning*[a]

Received 00th January 20xx,
Accepted 00th January 20xx

DOI: 10.1039/x0xx00000x

Quantum dot light emitting diode (QLED) is rising as a promising light emitting technology. However, the widely used insulative organic ligands hamper carriers injection. Herein, we developed a bi-inorganic-ligands strategy to replace organic ligands and dispersed QDs in a benign solvent butylamine. The all-inorganic QD film shows enhanced luminescent intensity, superior thermal stability and conductivity. In the end, we exploited the first prototype all inorganic QLED.

The narrow emission peak, high photoluminescence quantum yield (PL QY), size-dependent bandgap tunability, and solution processability of colloidal quantum dots (QDs) make them ideal materials for light emitting diodes and lasers.[1, 2] The performance of QD-based light emitting diodes (QLED) has been significantly improved in recent years via QD structure manipulation,[3, 4] surface ligand engineering,[5, 6] and device structure manipulation.[7]

Almost all QLEDs are based on QDs with organic ligands such as alkyl molecules with acid or thiol groups. These QD films show high luminescent quantum yield. However, the insulating molecules could hamper carriers injection, bringing low current density and luminescence intensity. Especially, this has been a bottleneck that limited the development of electrical pumped laser based on QDs. Furthermore, the weakly coordinated organic ligands can desorb under electrical field boiling, leading to the formation of dangling bond and deterioration of device performance.

In comparison to organic ligands, inorganic ligands can improve conductivity and stability of the QD films.[8-12] Inorganic ligands were used for QD solar cells and greatly enhanced the efficiency and stability of this kind of solar cells. [8-13] Very recently, inorganic ligand was explored for QLEDs base on solid-state ligand exchange.[6] However, to the best of our knowledge, there are no reports of using QD ink based inorganic ligands for QLEDs. Firstly, inorganic ligands coordinated QDs generally are dispersed in high polarity solvent with high boiling temperature, which makes it difficult to fabricate QD films. Secondly, the strong interaction between solvent and ligands typically brings ligand loss during film fabrication and gives rise to the low PL QY in the solid state.

Herein, we explored hydroxide and sulfide bi-ligands to coordinated QD surface, which enabled QDs to be dispersed in low polarity solvent. This significantly reduced the interaction force between solvent and ligands and alleviated ligand loss during film fabrication, giving rise to much-enhanced luminescence intensity. The conductivity of the inorganic ligand coordinated QD film is one order of magnitude improved and it shows superior thermal stability. In the end, by using ZnO and NiO as the electron and hole transporting layers respectively, we constructed, for the first time, a prototype all inorganic QLED.

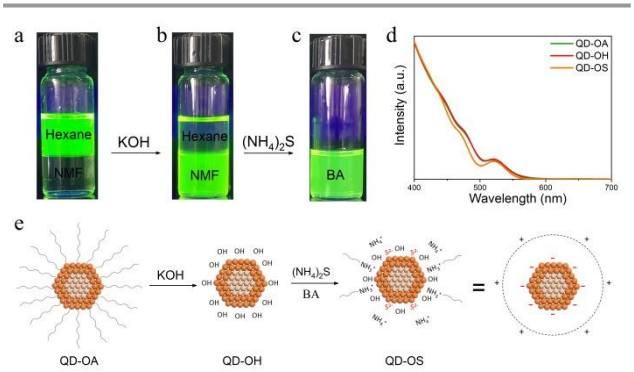

Figure 1. Photographs of QD before (a) and after (b) ligand exchange under UV light. (c) Photograph of QD dissolved in BA under UV light. (d) Absorption spectra of QDs. (e) Schematic illustration of ligand exchange and dissolution in BA with the addition of $(NH_4)_2S$.

Solution phase ligand exchange was used to prepare the inorganic ligands coordinated QD ink. Chemical-composition-gradient CdSe@ZnS core-shell QDs were synthesized by a typical hot injection method.[14] QDs capped with oleic acid ligands (QD-OA) dispersed in

[a] *School of Physical Science and Technology, ShanghaiTech University, Shanghai 201210, China.*
[b] *Ming Hsieh Department of Electrical Engineering, University of Southern California, Los Angeles, CA 90089, USA.*
* *Corresponding author.*
‡ *These authors contributed equally.*
Electronic Supplementary Information (ESI) available: [details of any supplementary information available should be included here]. See DOI: 10.1039/x0xx00000x

hexane were mixed with N-methylformamide (NMF) containing KOH (**Figure 1a**). After a few minutes, the QDs were transferred into NMF phase (**Figure 1b**), indicating ligand exchange of the alkyl chain with OH, and we name it QD-OH.[8] The ligand-exchanged QDs were then separated via the addition of acetonitrile as an anti-solvent and subsequently dispersed in solvent for film fabrication (**Figure 1c**).

The use of solvent with low boiling temperature and polarity for QD ink facilitates film fabrication. Here we utilized butylamine (BA) as the solvent for film fabrication.[15] The exchanged QDs can't be dispersed in BA directly, while the addition of $(NH_4)_2S$ significantly increases the solubility, enabling the formation of a non-scattering solution (**Figure S1c, d**). A possible mechanism is proposed in **Figure 1e**. Due to their strong bonding strength of cadmium with sulfide anions, $(NH_4)_2S$ can replace a fraction of OH groups on the QD surface, the ligand exchanged QDs were named QD-OS. The bivalent sulfide ions offer a negative charge to attract ammonium cations, as evidenced by the existence of S^{2-} by X-ray photoelectron spectroscopy (XPS) measurement (**Figure 5b**, blue line). Meanwhile, the proton exchange between NMF and BA enables the formation of butylammonium, as indicated by ^{1}H nuclear magnetic resonance (^{1}H NMR) spectra (**Figure S2**).[16] Butylammonium can be attracted by anions on QD surface. Therefore, an electric double layer, consists of S^{2-}, NH_4^+ and short chain butylammonium is formed, which repels the aggregation of QDs. Furthermore, butylammonium on QD surface brings a steric hindrance to prevent approach of QDs.

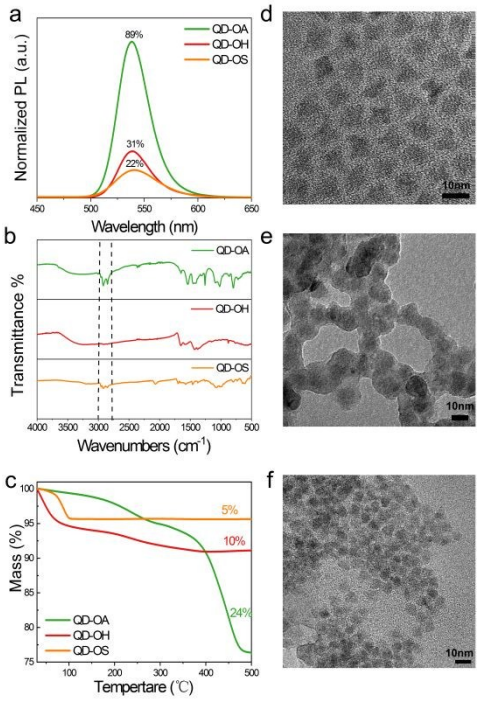

Figure 2. (a) PL spectra and PL QY of CdSe@ZnS QDs. (b) FTIR spectra of QDs. (c) Thermogravimetric analyses of QDs. (d-f) The TEM image of QD-OA, QD-OH, and QD-OS.

We then tested the photophysical properties of QDs. The QD-OA exhibits a high PL QY of 89% in hexane, while the PL QY decreases to 31% for QD-OH and 22% for QD-OS (**Figure 2a**). No obvious shift of the exciton peak position is observed in the absorption (Abs) spectra (**Figure 1d**), indicating that the size of QDs is maintained. Transmission electron microscopy (TEM) images show that the distance between QDs is reduced when OH ligands are used, ascribing to the smaller size of the inorganic ligands relative to the organic ligands (**Figure 2d, 2e**). The aggregation of QD-OH could be caused by the burning of unremoved high boiling temperature solvent NMF on QD surface. Boundaries of QDs are clearly observed for QD-OS (**Figure 2f**), indicating that the shapes of QDs are maintained well.

We then analysed the composition of QD surface in the films fabricated by spin coating using BA or NMF as solvents respectively. The residual organic ligands of the QD films are analysed by Fourier transform infrared spectroscopy (FTIR). The disappearance of the C-H stretching frequency (2800−3000 cm^{-1}) for the film prepared with QD-OH confirms that the organic ligands are substituted by OH ligands (**Figure 2b**).[17] Furthermore, thermogravimetric analysis (TGA) shows a 10% total weight loss for QD-OH, much lower than the 24% weight loss for QD-OA (**Figure 2c**). The weight loss of QD-OH can be ascribed to the remaining NMF solvent in the film. For the film made with QD-OS, transmission peak at 2800-3000 cm^{-1} in the FTIR spectrum is weak as well, and only a 5% (orange line) weight loss is observed, illustrating only a small amount of BA ligands remains in the film.

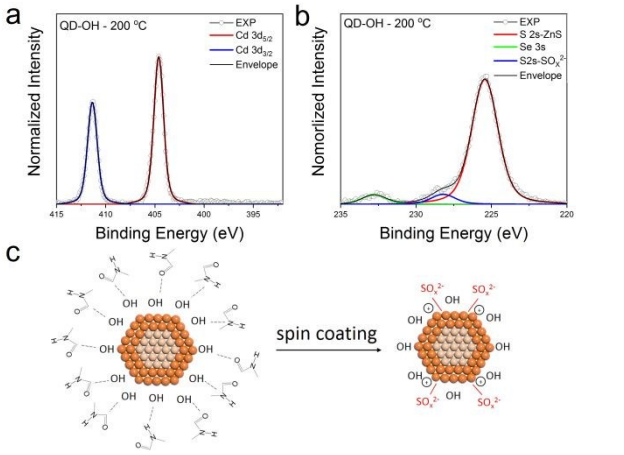

Figure 3. High-resolution Cd 3d (a) and S 2s (b) XPS spectra of the QD-OH with 200 ℃ annealing, EXP is the original data. (c) Scheme of the ligand-solvent interaction, ligand loss and QDs oxidized.

The use of NMF as solvent causes defects on QD surface. For the film prepared by QD-OH, a shoulder peak at 228.2 eV (**Figure 3b**) corresponding to the S 2s peak from SO_X^{2-} is observed, indicating the oxidation of QDs (**Figure 3c**).[18] Most probably the oxidation occurs at QD surface, since the steric hindrance for the atoms inside prevent the reaction. SO_X^{2-} groups are known to result in the formation of deep energy level trap states, bringing the decrease of emission intensity. In contrast, the peak belonging to SO_X^{2-} is not found for the film that fabricated from QD-OS. Furthermore, the atomic ratio of OH to Zn is 62.5% for the film made by QD-OH, while it is 92% for QD-OS (**Table S1, Figure S3**), indicating that the amount of OH ligand for the film prepared by QD-OH is much less than that by QD-OS. The loss of ligands contributes to the formation of defects on QD surface. Non-radiative recombination at defects as well as the

energy transfer between QDs and 'bad' dots with numerous trap states bring the decrease of PL QY.[19] The PL QY of the QD-OS film is 19%, much higher than that of QD-OH (9%) (**Figure S4**).

We then analysed the possible mechanism for the loss of ligands on QD surface. When two polar molecules close to each other, the negative ends will attract the positive ends of the other molecule and this is so called dipole-dipole force,[20, 21] a kind of van der Waals force. Owing to its large dipole moment, NMF strongly attracts OH ligands. Hence, when we removing solvent in film fabrication, it will cause the loss of ligands on QD surface simultaneously (**Figure 3c**). The use of low polarity solvent BA alleviated intermolecular forces between QDs, thereby suppressed ligand loss and surface oxidation.

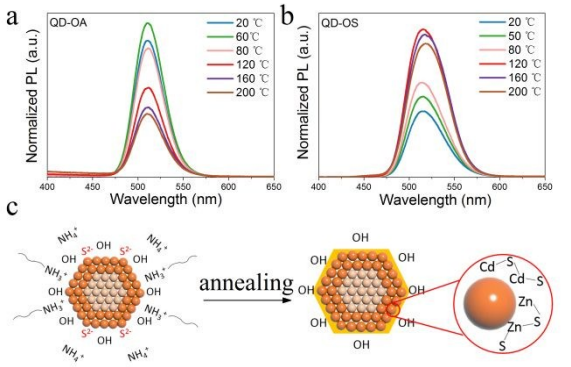

Figure 4. PL study of films fabricated from QD-OA (a) and QD-OS (b) with different annealing temperatures. (c) Schematic of the surface evolution via annealing.

The inorganic ligands capped QDs film shows excellent thermal stability. For the QD-OA film, the PL intensity decreased as increasing the annealing temperature (**Figure 4a, S5, Table S2**), most probably due to ligand desorption and the formation of dangling bonds on the QD surface. In contrast, PL intensity of the QD-OS film increased upon increasing annealing temperature (**Figure 4b, S5, Table S2**). However, it needs to be noted that the PL QY of the film after annealing is still lower than that with oleic acid.

XPS measurement was performed to analyse the mechanism for the enhanced thermal stability and PL intensity. The N 1s peaks at 402.1 eV and 400.1 eV are ascribed to NH_4^+ and BA groups, respectively (**Figure 5a**).[22] As the annealing temperature increased to 200 ℃, the N 1s peaks in XPS spectra disappeared, indicating that organic ligands on the QDs surface were removed. The S 2s peaks at 225.9 eV and 227.9 eV are ascribed to ZnS (**Figure 5b**, red line) and S^{2-} (blue line), respectively. After annealing, S 2s of S^{2-} and Se 3s peaks were disappeared, which can be attributed to the formation of CdS and ZnS shells,[23] since it removed the charges of S^{2-} and blocked photoelectron emission from the inner CdSe in XPS measurement (**Figure 4c**). The formation of CdS and ZnS shells passivates the surface dangling bonds and brings slight redshift of PL peak. The PL intensity increase of QD-OS might because of the formation of well-passivated shell structures and the corresponding lower defect density.

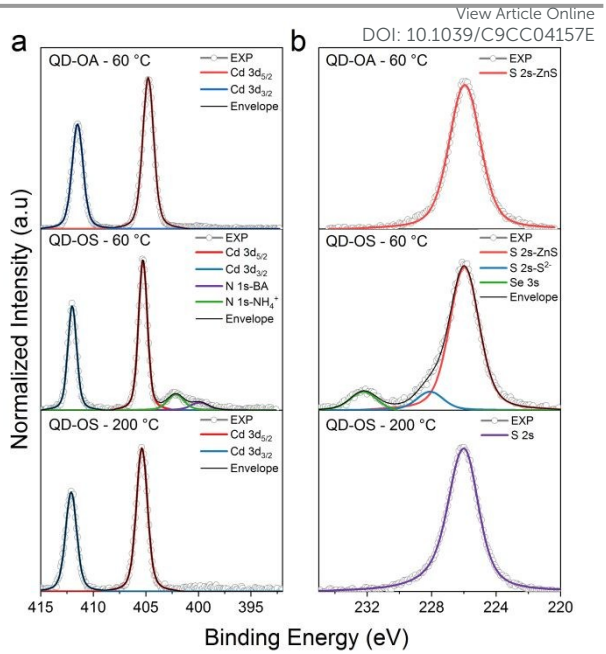

Figure 5. High-resolution Cd 3d, N 1s (a) and S 2s (b) XPS spectra of QD-OA with annealing at 60 °C, QD-OS with annealing at 60 ℃, and QD-OS with annealing at 200 ℃. EXP is the original data.

We fabricated QLED with chalcogenide-ligand-capped QDs. An inverted device structure was utilized employing NiO and ZnO as the hole and electron transport layer respectively, and an ultrathin passivating Al_2O_3 layer between NiO and QDs.[24] The band diagram of this structure is shown in **Figure 6a** using the work function reported.[25]

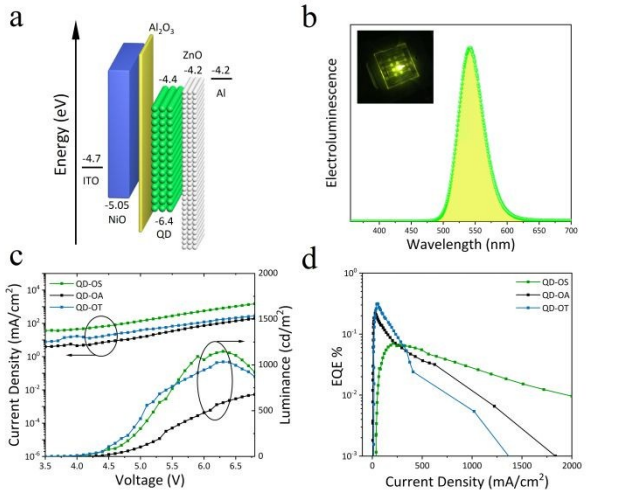

Figure 6. (a) Energy level diagram of the QLED. (b) EL spectrum of the corresponding device; inset: a photo of the operating device. (c) J-V-L plot and (d) EQE plot of QLED based on QD-OS, QD-OA and QD-OT.

The QLED based on QD-OS shows an electroluminescence (EL) peak at 541 nm with a full width half maximum value of approximately 45 nm (**Figure 6b**). The device shows one order of magnitude higher current density compared to OA and 1-Octanethiol (OT) capped control device (**Figure 6c**), which indicates its better conductivity. The

all-inorganic QLED exhibits a saturated green colour with luminance of 1149 cd m^{-2}, higher than those of the devices based on QD-OA and QD-OT (**Figure 6c**). Moreover, the organic-ligands-capped device break-down in high current region, while all-inorganic device shows good tolerance of high current (**Figure S6**). However, due to the much enhanced current density, the external quantum efficiency (EQE) of all-inorganic devices (0.07%) is lower than the organic one (0.22% of OA, 0.32% of OT) (**Figure 6d**).

In this report, we exploited hydroxide and sulfide mixed chalcogenide ligands to replace organic ligands on CdSe@ZnS QDs. The presence of mixed ligands on the QD surface reduces QDs aggregation and allows dispersal of QDs in a benign solvent BA. Alleviating the interaction between the solvent and ligands suppresses ligand desorption and surface oxidation. As a result, a luminescent QD film with chalcogenide ligands was realized, and the QD film can maintain its photoluminescence intensity even at an annealing temperature of 200 ℃. Finally, for the first time, we prepared a QLED based on all-inorganic-ligand-capped QDs that shows enhanced current density and luminescence intensity in comparison to those devices based on organic-ligand-capped QDs.

This work was supported by the Shanghai International Cooperation Project (16520720700), Shanghai Key Research Program (16JC1402100), ShanghaiTech Start-up Funding, 1000 Young Talent Program, National Natural Science Foundation of China (U1632118, 21571129), and Centre for High-resolution Electron Microscopy (*ChEM*), SPST, ShanghaiTech University under contract No. EM02161943. The authors also thank the Test Center of Shanghai Tech University and Dr. Peihong Cheng.

Conflicts of interest

There are no conflicts to declare.

Notes and references

1. V. Wood and V. Bulovic, *Nano Rev*, 2010, **1**.
2. Y. Q. Shang and Z. J. Ning, *Natl Sci Rev*, 2017, **4**, 170-183.
3. Y. Yang, Y. Zheng, W. Cao, A. Titov, J. Hyvonen, J. R. Manders, J. Xue, P. H. Holloway and L. Qian, *Nature Photonics*, 2015, **9**, 259-266.
4. Z. F. He, Y. Liu, Z. L. Yang, J. Li, J. Y. Cui, D. Chen, Z. S. Fang, H. P. He, Z. Z. Ye, H. M. Zhu, N. N. Wang, J. P. Wang and Y. Z. Jin, *Acs Photonics*, 2019, **6**, 587-594.
5. J. Pan, Y. Q. Shang, J. Yin, M. De Bastiani, W. Peng, I. Dursun, L. Sinatra, A. M. El-Zohry, M. N. Hedhili, A. H. Emwas, O. F. Mohammed, Z. J. Ning and O. M. Bakr, *Journal of the American Chemical Society*, 2018, **140**, 562-565.
6. X. Li, Y.-B. Zhao, F. Fan, L. Levina, M. Liu, R. Quintero-Bermudez, X. Gong, L. N. Quan, J. Fan, Z. Yang, S. Hoogland, O. Voznyy, Z.-H. Lu and E. H. Sargent, *Nat Photonics*, 2018, **12**, 159-164.
7. X. Dai, Z. Zhang, Y. Jin, Y. Niu, H. Cao, X. Liang, L. Chen, J. Wang and X. Peng, *Nature*, 2014, **515**, 96-99.
8. A. Nag, M. V. Kovalenko, J. S. Lee, W. Liu, B. Spokoyny and D. V. Talapin, *J Am Chem Soc*, 2011, **133**, 10612-10620.
9. Z. Ning, X. Gong, R. Comin, G. Walters, F. Fan, O. Voznyy, E. Yassitepe, A. Buin, S. Hoogland and E. H. Sargent, *Nature*, 2015, **523**, 324-328.
10. M. V. Kovalenko, M. Scheele and D. V. Talapin, *Science*, 2009, **324**, 1417-1420.
11. S. Kim, A. R. Marshal, D. M. Kroupa, E. M. Miller, J. M. Luther, S. Jeong and M. C. Beard, *Acs Nano*, 2015, **9**, 8157-8164.
12. G. P. Li, J. S. Huang, Y. Q. Li, J. X. Tang and Y. Jiang, *Nano Res*, 2019, **12**, 109-114.
13. Z. Ning, O. Voznyy, J. Pan, S. Hoogland, V. Adinolfi, J. Xu, M. Li, A. R. Kirmani, J.-P. Sun, J. Minor, K. W. Kemp, H. Dong, L. Rollny, A. Labelle, G. Carey, B. Sutherland, I. G. Hill, A. Amassian, H. Liu, J. Tang, O. M. Bakr and E. H. Sargent, *Nature Materials*, 2014, **13**, 822-828.
14. W. K. Bae, J. Kwak, J. W. Park, K. Char, C. Lee and S. Lee, *Advanced Materials*, 2009, **21**, 1690-1694.
15. Z. J. Ning, H. P. Dong, Q. Zhang, O. Voznyy and E. H. Sargent, *Acs Nano*, 2014, **8**, 10321-10327.
16. V. Sayevich, C. Guhrenz, V. M. Dzhagan, M. Sin, M. Werheid, B. Cai, L. Borchardt, J. Widmer, D. R. Zahn, E. Brunner, V. Lesnyak, N. Gaponik and A. Eychmuller, *Acs Nano*, 2017, **11**, 1559-1571.
17. A. Dong, X. Ye, J. Chen, Y. Kang, T. Gordon, J. M. Kikkawa and C. B. Murray, *J Am Chem Soc*, 2011, **133**, 998-1006.
18. G. Gabka, P. Bujak, K. Giedyk, K. Kotwica, A. Ostrowski, K. Malinowska, W. Lisowski, J. W. Sobczak and A. Pron, *Phys Chem Chem Phys*, 2014, **16**, 23082-23088.
19. N. J. L. K. Davis, J. R. Allardice, J. Xiao, A. Karani, T. C. Jellicoe, A. Rao and N. C. Greenham, *Mater Horiz*, 2019, **6**, 137-143.
20. R. Klajn, K. J. Bishop and B. A. Grzybowski, *Proc Natl Acad Sci U S A*, 2007, **104**, 10305-10309.
21. T. Wang, D. LaMontagne, J. Lynch, J. Zhuang and Y. C. Cao, *Chem Soc Rev*, 2013, **42**, 2804-2823.
22. J. J. Park, S. H. Lacerda, S. K. Stanley, B. M. Vogel, S. Kim, J. F. Douglas, D. Raghavan and A. Karim, *Langmuir*, 2009, **25**, 443-450.
23. H. Zhang, B. Hu, L. Sun, R. Hovden, F. W. Wise, D. A. Muller and R. D. Robinson, *Nano Lett*, 2011, **11**, 5356-5361.
24. W. Ji, H. Shen, H. Zhang, Z. Kang and H. Zhang, *Nanoscale*, 2018, **10**, 11103-11109.
25. B. S. Mashford, T. L. Nguyen, G. J. Wilson and P. Mulvaney, *J Mater Chem*, 2010, **20**, 167-172.